

Systematic study of direct neutron capture

Yi Xu and Stephane Goriely

Institut d'Astronomie et d'Astrophysique, C.P. 226, Université Libre de Bruxelles, Boulevard du Triomphe, B-1050 Brussels, Belgium

(Received 19 July 2012; published 22 October 2012)

The direct neutron capture reaction is investigated within the potential model. All allowed electric dipole ($E1$), electric quadrupole ($E2$), and magnetic dipole ($M1$) transitions are taken into account. The nuclear structure ingredients involved in the calculation are determined from experimental data whenever available, and if not, from global microscopic nuclear models. A special emphasis is put on the excitation spectrum deduced from a mean field plus combinatorial model of nuclear level densities. It is shown that considering either a total intrinsic nuclear level density or one-particle, one-hole neutron excitations give rise to similar predictions provided the corresponding average spectroscopic factor is renormalized. The potential model is shown to provide a fair agreement between the predicted radiative neutron capture cross section and experimental data for light targets as well as with previous calculations. A systematic study for about 6400 nuclei with $8 \leq Z \leq 102$ lying between the proton and neutron drip lines shows that the direct capture cross sections (and consequently reaction rates of astrophysical interest) are proportional to the number of levels available below the neutron threshold and decreases with decreasing neutron separation energies. It is found that the $E2$ and $M1$ components are usually negligible with respect to the $E1$ contribution, but that they can dominate the direct capture rate for about several hundred nuclei.

DOI: [10.1103/PhysRevC.86.045801](https://doi.org/10.1103/PhysRevC.86.045801)

PACS number(s): 24.10.-i, 24.50.+g, 25.60.Tv, 26.30.-k

I. INTRODUCTION

Nuclear reactions of astrophysical interest often concern unstable or even exotic species for which no experimental data exist. Although significant efforts have been devoted in the past decades, experimental information covers only a minute fraction of the entire data set required for nuclear astrophysics. Moreover, the energy range for which experimental data are available is restricted to the small range that can be studied by present experimental setups. For all cases, only theoretical predictions can fill the gaps. One of these specific examples concerns the rapid neutron-capture process (or r process) called for to explain the origin of about half of the elements heavier than iron observed in nature (for a review, see Ref. [1]). The r process is believed to take place in environments characterized by the high neutron densities, such that successive neutron captures can proceed into neutron-rich regions well off the β -stability valley. It involves a large number (typically 5000) of unstable nuclei for which many different properties have to be determined and cannot be obtained experimentally. One such fundamental property concerns the radiative neutron capture reaction.

So far, the neutron capture rates are usually evaluated within the statistical Hauser-Feshbach (HF) model [2]. The model makes the fundamental assumption that the capture process takes place with the intermediary formation of a compound nucleus (CN) in thermodynamic equilibrium. The energy of the incident particle is then shared more or less uniformly by all the nucleons before releasing the energy by particle emission or γ deexcitation. The formation of a CN is usually justified by assuming that the level density in the CN at the projectile incident energy is large enough to ensure an average statistical continuum superposition of available resonances [3]. However, when the number of available states in the compound system is relatively small, the validity of the HF

predictions has to be questioned, the neutron capture process being possibly dominated by direct electromagnetic transitions to a bound final state rather than through a CN intermediary. The direct capture (DC) proceeds via the excitation of only a few degrees of freedom on a much shorter time scale, reflecting the time taken by the projectile to traverse the target. For the DC process, the mean free path of the incident particle is comparable with the size of the nucleus and the particle ejection occurs preferentially at forward angles. It has become clear, however, that the DC process is important, and often dominating at the very low energies of astrophysical interest (e.g., Ref. [4]). Such DC reaction is known to play an important role for light or exotic nuclei systems for which few, or even no resonant states are available [5,6]. Between these two extreme CN and DC cases lies the so-called pre-equilibrium (PE) process characteristic of high-energy collisions where particles can be emitted after the first direct interaction and before the statistical equilibrium can be reached.

The CN, PE, and DC contributions to nuclear reactions are known to be not mutually exclusive. All mechanisms may contribute to the radiative capture of a neutron. For this reason, the total cross section is usually taken as the simple sum of these contributions, neglecting all possible interferences between them. The CN and PE contributions to the neutron capture reaction have been thoroughly studied and can be calculated, for example, within the modern reaction code TALYS [2] for which all the nuclear structure properties are taken from experimental information or state-of-the-art nuclear models. In contrast, the DC process, although widely used for nucleon capture on light target has only rarely been applied systematically to heavy neutron-rich nuclei.

It has been shown through a simple analytical model [7] that the DC contribution may dominate the total cross section for closed neutron shells (neutron-magic) targets or targets with a low neutron binding energy. For these nuclei, the number of

available resonances is very limited, restricting accordingly the CN contribution. In general, the CN contribution is by far dominant for nuclei close to the valley of stability and decreases rapidly when considering more and more neutron-rich nuclei (especially when crossing a magic neutron number), while the DC contribution remains. In Ref. [8], it was found that the DC mechanism is often not negligible compared with the CN process for nuclei close to the valley of stability and that neutron-rich nuclei present DC rates which show large variations according to the allowed or forbidden $E1$ transitions available between the initial and final systems. Large uncertainties obviously still affect the DC predictions, but the results found in Ref. [8] (based on the potential model including the $E1$ transitions only) also emphasize the possibility of a negligible DC rate for many neutron-rich nuclei.

In this paper, a new systematic calculation of the neutron DC reaction is performed. It represents an extension of the work of Ref. [8] based on the potential model, in which in addition to the electric dipole ($E1$) contribution, also the electric quadrupole ($E2$) and magnetic dipole ($M1$) transitions are calculated, as described in Sec. II. Nuclear structure ingredients used in the potential model calculation are detailed in Sec. III, where special emphasis is put not only on the neutron-nucleus interaction potential, but also on the excitation spectrum deduced from a recent combinatorial model of nuclear level densities (NLD). Results are discussed in Sec. IV, including the comparison between model predictions and experimental data, the prediction of the neutron DC reaction rates for about 6400 nuclei with $8 \leq Z \leq 102$ lying between the proton and neutron drip lines, and the explicit analysis of each of the $E1$, $E2$, and $M1$ contributions to the total neutron DC reaction rates. Finally, we summarize the results in Sec. V.

II. THE POTENTIAL MODEL

Different approaches exist for describing the low-energy nuclear reactions of astrophysical interest. What may be considered as two extremes are the R -matrix method on the purely phenomenological side and microscopic models such as the resonating group method or the generator coordinate method on the more fundamental side. These methods have been subject to large scrutiny in the last decades. Between these two extremes lies the potential model. More details on these models can be found in Refs. [4,9,10].

As a perturbative approach, the potential model is employed to study the neutron DC reaction $A(n, \gamma)B$ describing the transition from the initial scattering state $A+n$ to the final nucleus B with accompanying γ -ray emission. The allowed electric dipole ($E1$), electric quadrupole ($E2$), and magnetic dipole ($M1$) transitions to the ground state as well as all possible excited states in the final nucleus are taken into account. Many works on neutron capture reaction [8,11–13] have been devoted to the description of the DC reaction mechanism, in which the incoming neutron is scattered directly into a final bound state. When no experimental discrete level scheme exists, previous studies have tried to

predict the DC properties assuming one neutron particle-hole configuration deduced from the single-particle level scheme [14]. Unfortunately, this approach leads to large deviations between the predicted DC cross sections and experimental data because of the remarkable sensitivity of the cross section to the exact determination of the very few available final states. Moreover, different nuclear structure models inevitably give rise to different single-particle schemes, hence to considerable scattered predictions. To avoid such difficulties related to the discrete (or single-particle) level approach, we consider here the transitions to all possible energy levels, as described by the combination of nuclear discrete levels and a NLD model. In this way, the total DC cross section of a nucleus (Z, N) can be expressed as Ref. [8]

$$\sigma^{\text{DC}}(E) = \sum_{f=0}^x S_f \sigma_f^{\text{dis}}(E) + \langle S \rangle \int_{E_x}^{S_n} \sum_{J_f, \pi_f} \rho(E_f, J_f, \pi_f) \times \sigma_f^{\text{cont}}(E) dE_f. \quad (1)$$

In Eq. (1), E is the energy of the incident neutron and x corresponds to the last experimentally known level with excitation energy E_x (smaller than the neutron separation energy S_n). Below E_x , the sum of $\sigma_f^{\text{dis}}(E)$ runs over all the available discrete final states f (i.e., the experimental known energy levels). S_f is the spectroscopic factor, describing the overlap between the antisymmetrized wave function of the initial system $A+n$ and the final state f in B . Above E_x , the summation is replaced by a continuous integration over the spin (J)- and parity (π)-dependent NLD [$\rho(E, J, \pi)$] with the cross section $\sigma_f^{\text{cont}}(E)$ and the spectroscopic factor by an average quantity $\langle S \rangle$.

The potential model calculates the transition matrix element between the initial and the final states by sandwiching the electromagnetic operators in the long-wavelength limit. It is usually enough to consider the $E1$, $E2$, and $M1$ transitions, as discussed below. The final state f is either the ground state of the nucleus B if fed directly or, more generally, one of its excited states before the secondary γ -ray cascade. Correspondingly, we denote the total angular momentum and the parity of the initial $A+n$ system by J_i and π_i , and of the final state by J_f ($\equiv J_B$, spin of the nucleus B) and π_f . The spin-parity selection rules for the transition between these states can be expressed by a triangular relation $\mathbf{J}_i + \lambda = \mathbf{J}_f$, with λ being the multipolarity ($\lambda = 1$ for $E1$ and $M1$, $\lambda = 2$ for $E2$), and $\pi_i \pi_f$ negative for $E1$ and positive for $M1$ and $E2$.

The partial cross section $\sigma_f(E)$ to a given (discrete or continuum) final state f can be written as Ref. [9]

$$\begin{aligned} \sigma_f(E) &= \sigma_{J_f}^{\pi_f}(E) \\ &= \frac{2J_f + 1}{Ek(2J_A + 1)(2J_n + 1)} \sum_{I_f, J_i, l_i, J_i} \{c_1 k_\gamma^3 (|M_{E1}|^2 + |M_{M1}|^2) \\ &\quad + c_2 k_\gamma^5 |M_{E2}|^2\}, \end{aligned} \quad (2)$$

where $c_\lambda = (\lambda + 1)/\{\lambda[(2\lambda + 1)!!]^2\}$, J_A and J_n are the spin of the nucleus A and the neutron, respectively, and k_γ is the wave number of the emitted photon. The summations run over the channel spin I_i , orbital l_i , and total J_i angular momentum

of the initial state, and over the final channel spin I_f , provided that the spin-parity selection rules are fulfilled.

The matrix elements consist of two components related to the radial moments (\mathcal{M}_{E1} , \mathcal{M}_{E2} , \mathcal{M}_{M1}) and, if any, internal moments of the nucleus A [$\mathcal{M}_{M1}^{\text{int}}(A)$, $\mathcal{M}_{E2}^{\text{int}}(A)$] or neutron [$\mathcal{M}_{M1}^{\text{int}}(n)$, $\mathcal{M}_{E2}^{\text{int}}(n)$]:

$$\begin{aligned} M_{E1} &= \mathcal{M}_{E1}, \\ M_{M1} &= \mathcal{M}_{M1} + \mathcal{M}_{M1}^{\text{int}}(A) + \mathcal{M}_{M1}^{\text{int}}(n), \\ M_{E2} &= \mathcal{M}_{E2} + \mathcal{M}_{E2}^{\text{int}}(A) + \mathcal{M}_{E2}^{\text{int}}(n). \end{aligned} \quad (3)$$

The radial parts of the $E\lambda$ and $M1$ matrix elements are given by

$$\mathcal{M}_{E\lambda} = eZ_A \left(\frac{m_n}{m_A + m_n} \right)^\lambda \delta_{l_i l_f} C_\lambda^{i f} \langle l_i \lambda l_f | 000 \rangle \mathcal{I}_\lambda^{i f} \quad (4)$$

and

$$\mathcal{M}_{M1} = \frac{\mu_N Z_A m_n^2 \delta_{l_i l_f} \delta_{l_i l_f}}{m_A m_n (m_A + m_n)} \left(-C_1^{i f} \right) \sqrt{l_i(l_i + 1)} \mathcal{I}_0^{i f}, \quad (5)$$

where $\delta_{\kappa\kappa'}$ stands for the Kronecker symbol, $\langle | \rangle$ denotes the Clebsch-Gordan coefficients,

$$\begin{aligned} C_\lambda^{i f} &= (-)^{l_i + J_i + l_i} [(2\lambda + 1)(2J_i + 1)(2l_i + 1)/(4\pi)]^{1/2} \\ &\times \begin{Bmatrix} J_i & J_f & \lambda \\ l_f & l_i & I_i \end{Bmatrix}, \end{aligned} \quad (6)$$

and

$$\mathcal{I}_\nu^{i f} = \int \phi_{n l_f}(r) r^\nu \chi_{l_i}(E, r) dr. \quad (7)$$

In the above, the quantity with the curly brackets $\{ : : \}$ is the six- j symbol. An additional triangular relation $\mathbf{I}_i + \lambda = \mathbf{I}_f$ holds. $M_{E\lambda}$ vanishes when $l_i + l_f + \lambda$ is an odd number, and so does M_{M1} when $l_f = 0$.

The $E2$ and $M1$ matrix elements related to the internal moments of the nucleus A are

$$\begin{aligned} \mathcal{M}_{E\lambda}(A) &= \sqrt{5/4} Q_{2,A} \delta_{l_i l_f} D_\lambda^{i f} \mathcal{I}_0^{i f}, \\ \mathcal{M}_{M1}(A) &= \sqrt{3} \mu_{1,A} \delta_{l_i l_f} D_1^{i f} \mathcal{I}_0^{i f}, \end{aligned} \quad (8)$$

where $Q_{2,A}$ and $\mu_{1,A}$ are the electric quadrupole and the magnetic dipole moments of the nucleus A , respectively, as calculated in Sec. III A, and

$$\begin{aligned} D_\lambda^{i f} &= (-)^{J_A + J_n - I_f - l_f} [(2J_i + 1)(2J_A + 1)(2I_i + 1) \\ &\times (2I_f + 1)/(4\pi)]^{1/2} \times \begin{Bmatrix} J_i & J_f & \lambda \\ I_f & I_i & l_f \end{Bmatrix} \\ &\times \begin{Bmatrix} J_A & J_n & I_f \\ I_i & \lambda & J_A \end{Bmatrix} / \langle J_A \lambda J_A | J_A 0 J_A \rangle. \end{aligned} \quad (9)$$

Similar expressions of $\mathcal{M}_{E\lambda}(n)$ and $\mathcal{M}_{M1}(n)$ for the neutron can be deduced by switching the suffix A and n in Eqs. (8) and (9). For the internal terms, the additional triangular relation is $\mathbf{I}_i = \mathbf{I}_f - \lambda$.

In Eq. (7), the radial wave functions are obtained by solving the two-body Schrödinger equations, the radial parts of which may be expressed in the relative coordinate r as

$$\left[\frac{d^2}{dr^2} - \frac{L(L+1)}{r^2} + \frac{2\mu}{\hbar^2} \{E - V(E, r)\} \right] \psi = 0. \quad (10)$$

Here, $V(E, r)$ is an energy-dependent central nuclear potential, L is the relative orbital angular momentum, $\mu = m_A m_n / (m_A + m_n)$ is the reduced mass, and ψ represents the resulting radial wave function, which vanishes at the origin. For the sake of clarity, we renamed ψ by χ in the case of scattering problems ($E > 0$) and by ϕ in the case of the eigenvalue bound problems ($E < 0$) in Eq. (7).

For scattering states ($E = \hbar^2 k^2 / 2\mu$, where k is the wave number and μ the reduced mass), the radial wave functions $\chi_L(k, r)$ behave asymptotically at large distances as

$$\chi_L(k, r) \rightarrow e^{i\delta_L} [\cos(\delta_L) k r J_L(kr) - \sin(\delta_L) k r Y_L(kr)], \quad (11)$$

where δ_L is the phase shift of the elastic scattering by the nuclear potential, and $J_L(kr)$ and $Y_L(kr)$ are the Bessel functions of first and second kinds, respectively.

For bound states, the radial wave functions must vanish at infinity and be normalized as

$$\int_0^\infty |\phi_{nL}(r)|^2 dr = 1, \quad (12)$$

where n stands for the radial quantum number.

III. NUCLEAR INGREDIENTS

The nuclear inputs required for the potential model calculations, as described in the previous sections, can be extracted from basic nuclear structure properties. Whenever available, the nuclear ingredients are taken from experiment. If not, global models, as described below, are considered. For a reliable prediction, such models need to be as microscopic as possible, especially when dealing with exotic neutron-rich nuclei for which extrapolation is required.

A. Nuclear mass, electromagnetic multipole moments, and spectroscopic factor

Nuclear masses are taken from the 2011 Atomic Mass Evaluation [15] whenever available. Theoretical mass data are predicted by the Hartree-Fock-Bogoliubov (HFB) method based on the effective nucleon-nucleon interaction of Skyrme type, namely the HFB-21 mass model [16]. The nuclear magnetic dipole (μ_1) and electric quadrupole (Q_2) moments appearing in Eq. (8) are taken from the experimental data compilation [17]. When no data are available, the single-particle model is used for predicting the nuclear magnetic dipole moment, while the nuclear deformation (β_2) obtained within the HFB-21 calculation [16,18] is used to estimate the electric quadrupole moments.

So far, the determination of the spectroscopic factor remains a difficult problem. Closed-shell nuclei, or at low

excitation energy, often have discrete levels with a high-purity single-particle configuration. However, away from the magic numbers, or at increasing excitation energy, residual interactions and couplings of the single-particle motion to other degrees of freedom, distribute the spectroscopic strength of a single-particle state among several nuclear levels. The spreading and fragmentation of the single-particle states give a continuous spectroscopic strength if the fragmentation width is larger than the spacing of the single-particle states [19].

In our calculation, experimental spectroscopic factors compiled in Ref. [20] are included for the discrete level contributions in Eq. (1). For the discrete levels for which no experimental data exist, an average value $S_f = 0.347$ is adopted. This value corresponds to the average value from all the compiled experimental spectroscopic factors [20] for levels with allowed $E1$, $E2$, and $M1$ transitions. However, for theoretically determined levels, when pure neutron $1p1h$ excitations are considered here (see Sec. III C), the averaged spectroscopic factor $\langle S \rangle = 1$ is adopted. This estimate minimizes the deviation between the cross sections computed by Eq. (1) and the cross sections computed by

$$\sigma^{\text{DC}}(E) = \langle S \rangle \int_0^{S_n} \sum_{J_f, \pi_f} \rho(E_f, J_f, \pi_f) \sigma_f^{\text{cont}}(E) dE_f \quad (13)$$

for the nuclei for which experimental spectroscopic factors are available in Ref. [20] as well as for light nuclei for which the cross section has been measured (see Sec. IV). Equivalently, $\langle S \rangle = 1$ assumes that the experimental known level schemes are rather well described by the theoretical levels deduced from the adopted NLD model, as discussed below.

B. Nuclear potential

In the present calculation, we restrict ourselves to the so-called JLMB potential from the Bruyères-le-Châtel renormalization of the Jeukenne-Lejeune-Mahaux potential [21,22] to solve the Schrödinger equation of Eq. (10). More specifically, the energy-dependent $V_{\text{JLMB}}(E, r)$ is used in the entrance channel to generate the initial (scattering state) radial wave function χ , while the energy-independent $V_{\text{JLMB}}(r)(E=0)$ is used in the exit channel to generate the final (bound state) radial wave function ϕ . The JLMB nuclear potential is a semimicroscopic nucleon-nucleus spherical optical model potential which has been extended to deformed and unstable nuclei with $A = 30$ to 240 and for energies ranging from 10 keV up to 200 MeV [22–24]. In particular, the JLMB nuclear potential was phenomenologically renormalized in Refs. [22,25] to improve the agreement between experimental and predicted observables for a large set of experimental data.

The JLMB nuclear potential for a given nuclear matter density $\rho = \rho_n + \rho_p$ and asymmetry $\alpha = (\rho_n - \rho_p)/\rho$ reads

$$V(E, r) = \lambda_V(E)[V_0(E) + \lambda_{V1}(E)\alpha V_1(E)] \\ + i\lambda_W(E)[W_0(E) + \lambda_{W1}(E)\alpha W_1(E)], \quad (14)$$

with E the incident nucleon energy, and $V_0(E)$, $V_1(E)$, $W_0(E)$, and $W_1(E)$ are the real isoscalar, real isovector, imaginary isoscalar, and imaginary isovector nuclear potential

components, respectively, and $\lambda_V(E)$, $\lambda_{V1}(E)$, $\lambda_W(E)$, and $\lambda_{W1}(E)$ their respective renormalization factors. The HFB-21 matter density (ρ_n and ρ_p) [16,18] are used to calculate the four components of the JLMB nuclear potential in Eq. (14) on the basis of the local approximation applied to Brückner-Hartree-Fock calculation of nuclear matter [21,26]. The expressions for $\lambda_V(E)$, $\lambda_{V1}(E)$, $\lambda_W(E)$, and $\lambda_{W1}(E)$ can be found in Ref. [22].

As is classically assumed, we neglect in the present study the imaginary part of the potential, which is thought to give a negligible contribution to the total cross section for nuclei with low neutron separation energy, because of the small flux into reaction channels. It should also be stressed that cross sections calculated from various potentials are rather insensitive to their detailed form provided that they all have the same volume integral per nucleon (see, for example, Ref. [8]). Although few potentials are constructed to lead to good predictions of the volume integral, this requirement has been carefully kept in mind by Jeukenne *et al.* [21], who determined their potential to reproduce the experimental volume integrals and root-mean-square radii in a wide range of the periodic table.

Finally, note that the JLMB nuclear potential is also a popular choice made in CN capture calculations, especially for nuclear astrophysics applications (see, e.g., Ref. [2]). Assuming that both CN and DC mechanisms contribute to the neutron capture reaction, only a coherent treatment of both parts could ensure a reliable prediction of the total neutron capture cross sections.

C. Discrete level scheme and nuclear level density (NLD)

As shown by Eq. (1), nuclear level scheme is another crucial ingredient for the cross section calculation within the potential model. The discrete level schemes are taken

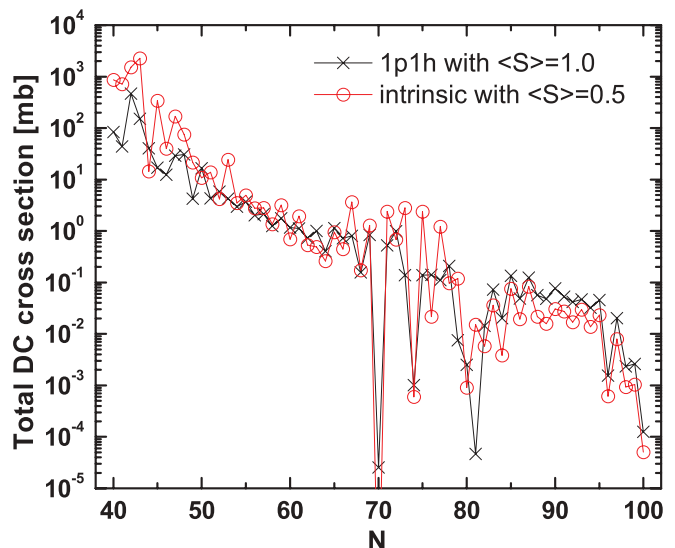


FIG. 1. (Color online) Comparison between the neutron DC cross sections computed by Eq. (1) with the neutron $1p1h$ NLD (crosses) and $\langle S \rangle = 1$ and those obtained with the total intrinsic NLD (circles) and $\langle S \rangle = 0.5$ for Sn isotopes at $E_n = 100$ keV.

from the RIPL-3 library [27]. It is well accepted that the predictions of DC potential model are in qualitatively good agreement with experimental results as long as all the details of the excitation spectrum are known experimentally [8,13,14]. However, when dealing with nuclei for which a complete set of experimental data is not available, large discrepancies can be expected. As a matter of fact, at least for light nuclei, the main contribution to the total DC cross section generally results from transitions to the ground state or to a small number of low-lying states, provided the selection rules allow for the considered electromagnetic transitions. The uncertainties related to the exact determination of the energy, spin, and parity of these levels can modify the DC contribution by many orders of magnitude. The selection rules depend on the exact spin and parity differences between the initial and final states and act as a real switch, turning on or off the DC reaction. The smaller the number of contributing levels, the larger the impact of an erroneous spin and parity affectation. In a similar way, the energy of the final state can also allow or forbid a transition according to its relative location with respect to the neutron separation energy S_n .

Owing to the high sensitivity of the cross section with respect to the energy, spin, and parity assignment of each excited level in the final nucleus, a special attention should be paid to the choice of the NLD model. In this situation, only a microscopic approach capable of estimating the non-statistical spin and parity dependence of the NLD, especially at low energies, should be considered [28,29]. Recently, a microscopic HFB plus combinatorial approach has proven its capacity to reproduce not only the low-lying cumulative number of levels but also the neutron resonance spacings at the neutron separation energy [30]. In the present calculation, the corresponding one-particle, one-hole (1p1h) neutron excitations deduced from exactly the same combinatorial NLD calculation is considered. Note that no collective enhancement is included in the NLD calculation to account for intrinsic single-particle excitations. In contrast to Ref. [8], where a total intrinsic (i.e., without collective enhancement) NLD was applied to Eq. (1) with a relatively low average spectroscopic factor ($\langle S \rangle = 0.1$), we consider here the neutron 1p1h excitations with a larger value of $\langle S \rangle = 1$ for each of these levels. As illustrated in Fig. 1, both approaches give rather similar predictions of the

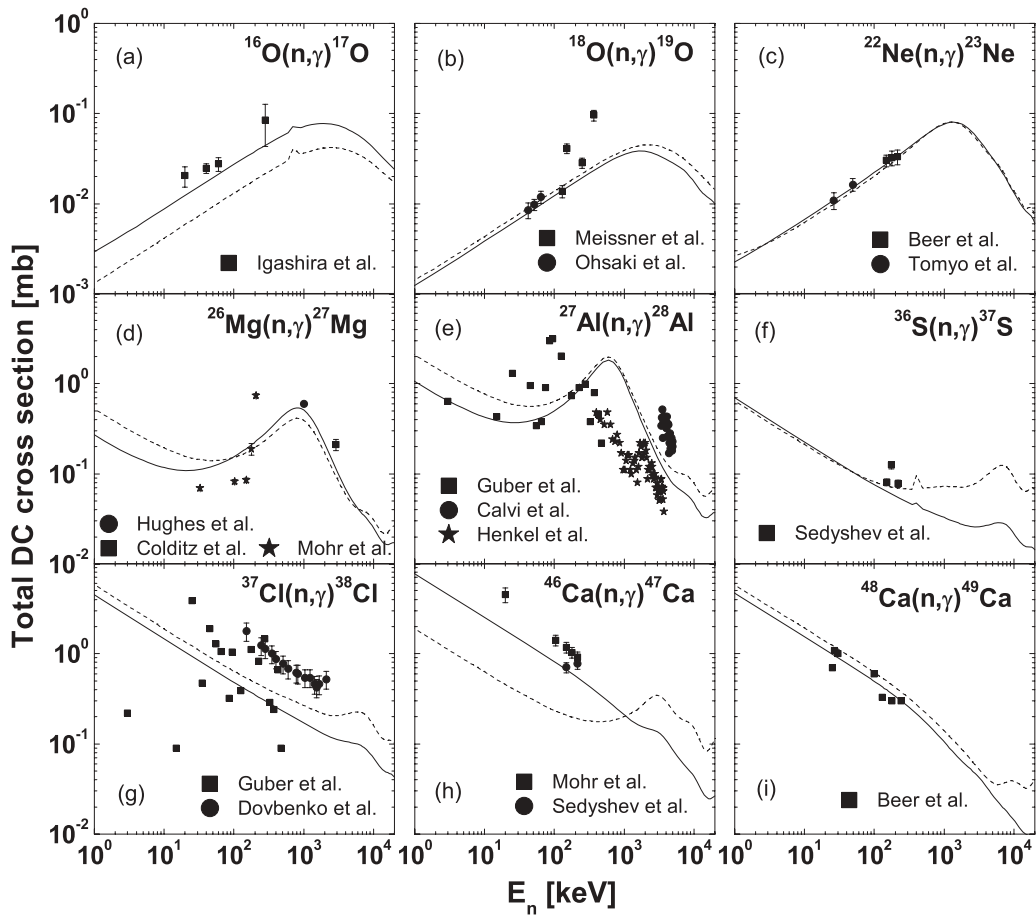


FIG. 2. Comparison of our calculated total neutron DC cross sections and the experimental data for 9 light nuclei. The solid lines correspond to the calculation by Eq. (1), including experimental discrete levels and known spectroscopic factors, while the dashed lines results from Eq. (13) with theoretical predictions only. Experimental data are taken from Ref. [31] for $^{16}\text{O}(n, \gamma)^{17}\text{O}$; Refs. [32,33] for $^{18}\text{O}(n, \gamma)^{19}\text{O}$; Refs. [34,35] for $^{22}\text{Ne}(n, \gamma)^{23}\text{Ne}$; Refs. [36–38] for $^{26}\text{Mg}(n, \gamma)^{27}\text{Mg}$; Refs. [39–41] for $^{27}\text{Al}(n, \gamma)^{28}\text{Al}$; Ref. [42] for $^{36}\text{S}(n, \gamma)^{37}\text{S}$; Refs. [39,43] for $^{37}\text{Cl}(n, \gamma)^{38}\text{Cl}$; Refs. [44,45] for $^{46}\text{Ca}(n, \gamma)^{47}\text{Ca}$; and Ref. [46] for $^{48}\text{Ca}(n, \gamma)^{49}\text{Ca}$.

DC cross section (at the energy $E_n = 100$ keV) for nuclei close to the valley of β stability, provided the average spectroscopic factor $\langle S \rangle = 0.5$ is adopted. For exotic n -rich Sn isotopes, the neutron separation energy is small and the proton excitations of low impact on the total NLD at such energies (in particular for a closed proton shell element like Sn), so that both approaches with the same value of the spectroscopic factor give similar results.

IV. RESULTS AND DISCUSSIONS

For light targets, the DC is known to give the main contribution to the total capture cross section, the resonant CN capture cross section being rather negligible. To test the reliability of the potential model, we compare in Fig. 2 our calculated neutron DC (including the $E1 + E2 + M1$ multipolarities) cross sections (solid lines) with the available experimental data for the nine neutron capture reactions on light nuclei, namely ^{16}O , ^{18}O , ^{22}Ne , ^{26}Mg , ^{27}Al , ^{36}S , ^{37}Cl , ^{46}Ca , and ^{48}Ca . A rather good agreement is found which confirms that the potential model with the adopted nuclear structure ingredients (in particular the average spectroscopic factor), as described in Sec. III, can provide a fair prediction of the neutron DC cross section. Note that for the open-shell heavy species like ^{36}S or ^{37}Cl the resonant capture already dominates the reaction mechanism, it is therefore not unrealistic to underestimate the experimental cross section. For the closed-shell Ca isotopes, the DC is still expected to dominate the reaction mechanism. Furthermore, to test the predictive power of the potential model, we compare in Fig. 2 the neutron DC cross section determined by Eq. (13) assuming no experimental data regarding the level scheme and spectroscopic factors is available. In this case, the neutron $1p1h$ NLD and an average spectroscopic factor $\langle S \rangle = 1$ are considered. Globally, the predictions remain rather satisfactory, the cross section being predicted within a factor of 2.

For both of the $^{122}\text{Sn}(n, \gamma)^{123}\text{Sn}$ and $^{132}\text{Sn}(n, \gamma)^{133}\text{Sn}$ reactions, our total neutron DC cross sections are compared in Fig. 3 with the predictions of Ref. [47] obtained also within the DC model (excluding the direct-semidirect contribution). A rather fair agreement between both calculations is found, keeping in mind that the nuclear ingredients may be rather different. Our higher cross section results from the transitions not only to the discrete experimental levels but also to the additional allowed high-lying levels deduced from the NLD.

The $E1$, $E2$, and $M1$ DC contributions to the Maxwellian-averaged reaction rate of astrophysics interest ($N_a \langle \sigma v \rangle$, where N_a is the Avogadro number, and v the relative velocity between target and projectile) are compared in Fig. 4 for the Sn isotopic chain. For most of the nuclei, the $E1$ component is larger than the $E2$ and $M1$ components by several orders of magnitude. However, in some cases, the $E1$ and $M1$ contributions can become comparable, for example, for ^{126}Sn . In many cases the $E2$ component becomes comparable with the $M1$ contribution, though it remains rather negligible with respect to the $E1$ contributions.

The neutron DC cross sections and reaction rates of astrophysics interest have been calculated for about 6400

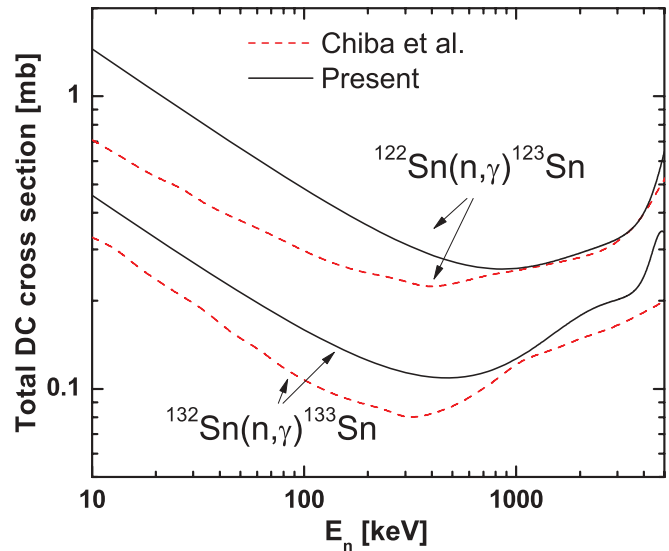


FIG. 3. (Color online) Comparison between the present total neutron DC cross section and the predictions of Ref. [47] for $^{122}\text{Sn}(n, \gamma)^{123}\text{Sn}$ and $^{132}\text{Sn}(n, \gamma)^{133}\text{Sn}$ reactions.

nuclei with $8 \leq Z \leq 102$ lying between the proton and neutron drip lines. Figure 5 shows the $E1$, $E2$, $M1$, and total neutron DC reaction rates represented in the (N, Z) plane of the target nuclei at $T_9 = 1$ (T_9 denotes the temperature in 10^9 K). One can see that, for all of $E1$, $E2$, $M1$, and total DC reaction rates, the neutron-deficient nuclides generally have larger cross sections in comparison with nuclei lying in the valley of β stability or on its neutron-rich side. Many neutron-rich nuclides close to the neutron drip line are also found to have a rather small DC cross section, which is mainly caused by the large decrease of the neutron separation energy and consequently the number of available levels at low energy. However, owing to the account of $E2$ and $M1$ transitions in addition to $E1$, the reaction rates are found to be always larger than typically

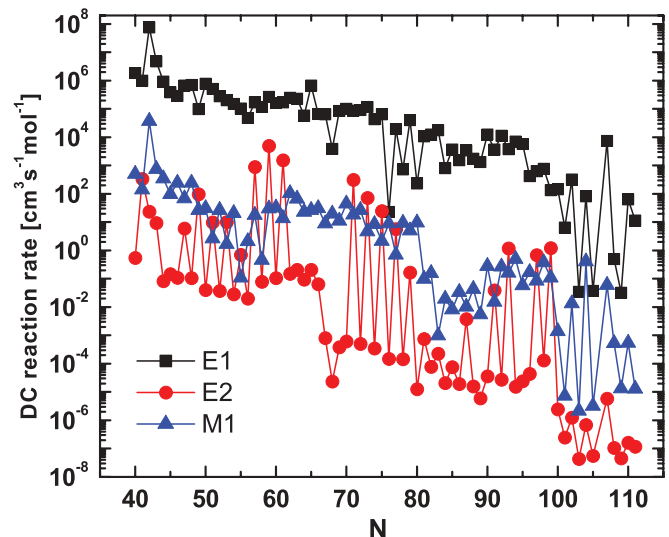


FIG. 4. (Color online) $E1$, $E2$, and $M1$ neutron DC reaction rates for Sn isotopes at $T_9 = 1$ (T_9 denotes the temperature in 10^9 K).

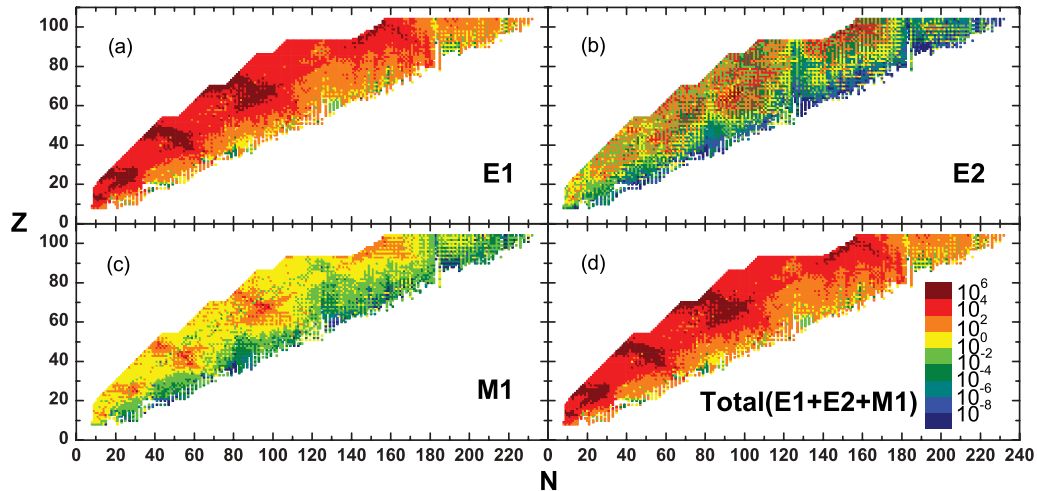


FIG. 5. (Color online) The $E1$, $E2$, $M1$, and total ($E1 + E2 + M1$) neutron DC reaction rates (in $\text{mol}^{-1} \text{cm}^3 \text{s}^{-1}$) represented in the (N, Z) plane at $T_9 = 1$.

$10^{-4} \text{mol}^{-1} \text{cm}^3 \text{s}^{-1}$, while in Ref. [8] it was found that for many nuclei, the $E1$ selection rules were not fulfilled and consequently a negligible DC rate was obtained.

The $E1$ and $M1$ contributions show some enhancements for target nuclei with a neutron number $N \simeq 20, 50, 90$, and 150 lying on the neutron-deficient side of the valley of β stability. In contrast, the $E2$ contribution presents a more scattered behavior. Targets with a high spin and electric quadrupole moment give rise to a correspondingly large $E2$ contribution (see also Fig. 6). It is rather obvious that for most nuclei the dominating contribution stems from the $E1$ transitions; this confirms previous calculations which neglected higher multiplicities [8].

Figure 6 shows the variation of the total ($E1 + E2 + M1$) neutron DC reaction rates with the neutron separation energy

(S_n) of the final nuclei at $T_9 = 1$. It is of particular interest to see that, in contrast to previous calculations [7], the present calculation predicts the cross section to decrease with decreasing S_n . This phenomenon is related to the number of excited levels below S_n , which decreases with decreasing S_n , leading to less possible transitions to the final states. Transitions to high-lying levels have a relatively small contribution to the total DC cross section owing to the small photon wave number k_γ in Eq. (2), but the exponentially rising number of levels with increasing excitation energy can compensate for this effect. Consequently, the total DC reaction rates are clearly proportional to the number of available levels, as already stressed in Ref. [8], and therefore do not necessarily depend on the transitions to low-lying states only. Figure 7 shows the variation of the total DC reaction rates with the neutron number $T_9 = 1$ and clearly

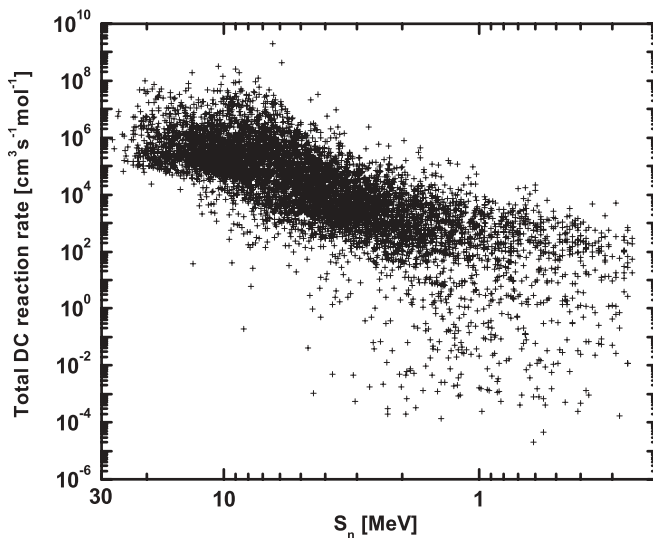


FIG. 6. Variation of the total ($E1 + E2 + M1$) neutron DC reaction rates with the neutron separation energy S_n of the final nuclei at $T_9 = 1$.

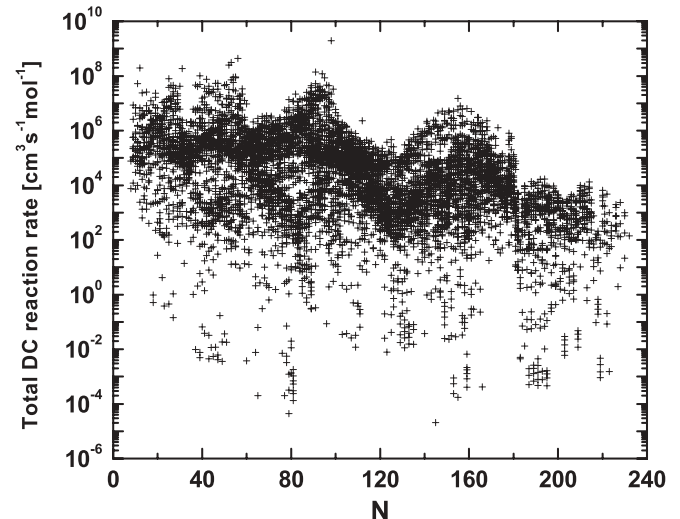


FIG. 7. Variation of the total ($E1 + E2 + M1$) neutron DC reaction rates with the neutron number N of the target nuclei at $T_9 = 1$.

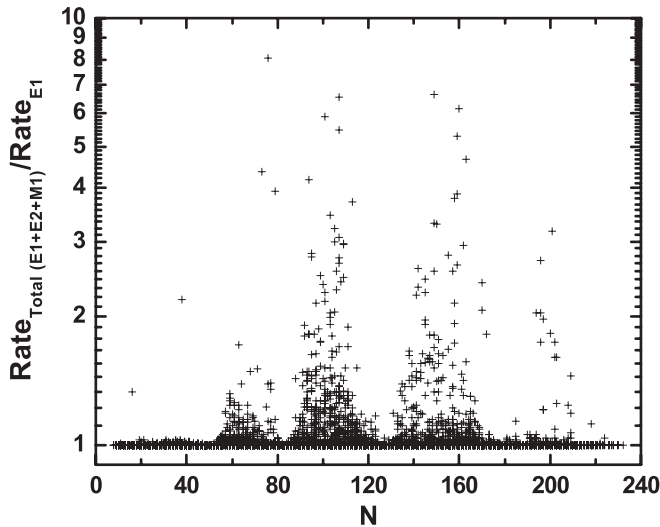


FIG. 8. Ratio of the total ($E1 + E2 + M1$) neutron DC reaction rate to the $E1$ rate as a function of the neutron number N at $T_9 = 1$.

illustrates the large DC rates at $N \simeq 20, 50, 90$, and 150 , as already observed in Fig. 5.

To analyze the possible contribution of the $E2$ and $M1$ transitions, the ratio of the total ($E1 + E2 + M1$) DC reaction rate to the $E1$ contribution at $T_9 = 1$ is shown in Fig. 8 for the same set of 6400 nuclei. Among those, a ratio larger than typically 1.2 is found for about 300 nuclei. For those nuclei, the $E2 + M1$ component is therefore comparable to the $E1$ component. The corresponding $E1$ and $E2 + M1$ DC rates are shown in Fig. 9 for those 300 nuclei. Such results contradict the idea that the $E2$ and $M1$ transitions are always negligible relative to the $E1$ transition. From Fig. 8, we also find that the target nuclei with large $M1$ and $E2$ rates usually have an open shell structure and lie close to the valley of β stability, as shown in Fig. 9. The enhancements of $E2$ and $M1$ components are attributed to (i) the allowed transitions to high-lying levels deduced from the NLD model and (ii) the internal parts of $E2$

and $M1$ transitions determined by the nuclear magnetic dipole (μ_1) and electric quadrupole (Q_2) moments [see Eq. (8)].

V. SUMMARY AND OUTLOOK

We have studied the neutron DC reactions on the basis of the potential model taking into account the $E1$, $E2$, and $M1$ allowed transitions to all possible final states, as found experimentally or deduced from a NLD model. The nuclear structure ingredients involved in the calculation, namely the nuclear mass, electromagnetic multipole moments, spectroscopic factor, neutron-nucleus interaction potential, and excited level scheme are determined from experimental data whenever available, and if not, from global microscopic nuclear models (except for the spectroscopic factors for which an average value is adopted). Such a combination of experimental data and model predictions allows not only for the essential coherence of the predictions for all experimental unknown data, but also a rather reliable extrapolation away from experimentally known energy or mass regions, as required in specific applications like nuclear astrophysics.

The present work represents an extension of the work of Ref. [8] based on the potential model, in which in addition to the electric dipole ($E1$) contribution, the electric quadrupole ($E2$) and magnetic dipole ($M1$) transitions are now also included. A special emphasis has also been put on the excitation spectrum deduced from a combinatorial model of NLD. It is shown that considering either a total intrinsic NLD or $1p1h$ neutron excitations give rise to similar predictions provided the corresponding spectroscopic factor is renormalized by a factor of 2.

We have shown that the potential model provides a fair agreement with experimental neutron capture cross sections for light targets as well as with previous calculations. A systematic study for about 6400 nuclei with $8 \leq Z \leq 102$ lying between the proton and neutron drip lines shows that the DC cross section decreases with increasing neutron richness,

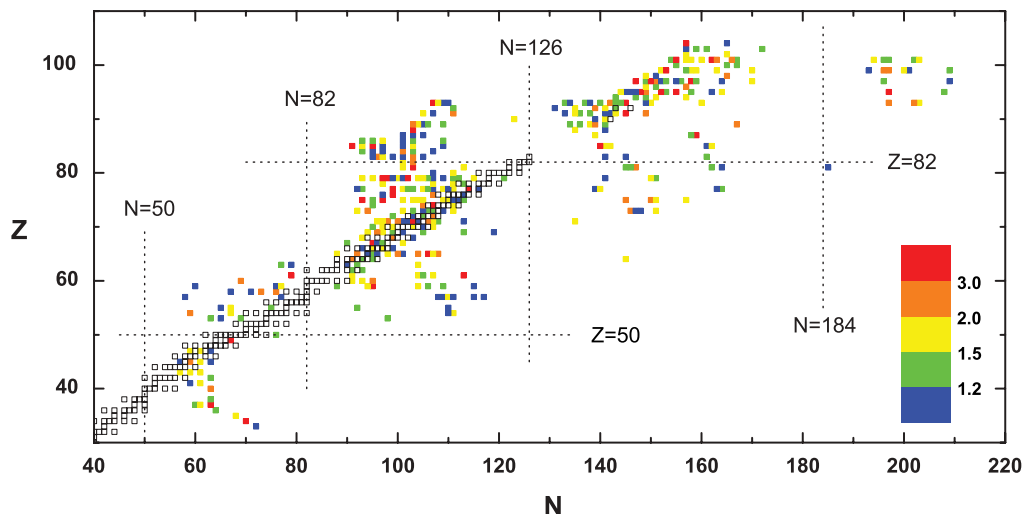


FIG. 9. (Color online) Representation in the (N, Z) plane of the total DC rate relative to the $E1$ contribution at $T_9 = 1$ for about the 300 nuclei with comparable $E1$ and $E2 + M1$ components, as shown in Fig. 8.

that is, with decreasing neutron separation energies. The DC cross section is clearly proportional to the number of available levels below the neutron threshold, as described by the combinatorial NLD model.

By comparing the ratio of the total ($E1 + E2 + M1$) DC reaction rates to the $E1$ contribution, it is found that the $E2$ and $M1$ components can significantly contribute to the DC rate for several hundred nuclei which usually have an open neutron shell structure. The additional transitions to the allowed high-lying levels (deduced from the NLD model), as well as the internal parts [Eq. (8)] of $M1$ and $E2$ transitions determined by the nuclear magnetic dipole (μ_1) and electric quadrupole

(Q_2) moments, are both responsible for these large $E2$ and $M1$ components.

The DC mechanism remains to be compared with the CN and PE components within one unique coherent framework based on the same nuclear structure models.

ACKNOWLEDGMENTS

This work has been supported by the Communauté Française de Belgique (Actions de Recherche Concertées). Y.X. acknowledges support for postdoctoral research from F.R.S.-FNRS. S.G. is a F.R.S.-FNRS Research Associate.

-
- [1] M. Arnould, S. Goriely, and K. Takahashi, *Phys. Rep.* **450**, 97 (2007).
- [2] S. Goriely, S. Hilaire, and A. J. Koning, *Astron. Astrophys.* **487**, 767 (2008).
- [3] G. R. Satchler, *Introduction to Nuclear Reactions* (Macmillan, New York, 1980).
- [4] H. Oberhummer and G. Staudt, in *Nuclei in the Cosmos*, edited by H. Oberhummer (Springer Verlag, Heidelberg, 1991), p. 29.
- [5] A. Mengoni, T. Otsuka, and M. Ishihara, *Phys. Rev. C* **52**, R2334 (1995).
- [6] H. Beer, C. Coceva, P. V. Sedyshev, Y. P. Popov, H. Herndl, R. Hofinger, P. Mohr, and H. Oberhummer, *Phys. Rev. C* **54**, 2014 (1996).
- [7] G. J. Mathews, A. Mengoni, F. K. Thielemann, and W. A. Fowler, *Astrophys. J.* **270**, 740 (1983).
- [8] S. Goriely, *Astron. Astrophys.* **325**, 414 (1997).
- [9] P. Descouvemont, *Theoretical Models for Nuclear Astrophysics* (Nova Science, New York, 2003).
- [10] P. Descouvemont, *J. Phys. G* **35**, 014006 (2008).
- [11] C. Rolfs, *Nucl. Phys. A* **217**, 29 (1973).
- [12] J. E. Lynn, *The Theory of Neutron Resonance Reactions* (Clarendon Press, Oxford, 1968).
- [13] G. R. Satchler, *Direct Nuclear Reactions* (Clarendon Press, Oxford, 1983).
- [14] H. Oberhummer, W. Balogh, R. Bieber, H. Herndl, U. Langer, T. Rauscher, and H. Beer, in *International Conference on Exotic Nuclei and Atomic Masses*, edited by M. de Saint Simon and O. Sorlin (Editions Frontières, Gif-sur-Yvette, 1995), p. 649.
- [15] G. Audi and W. Meng (private communication).
- [16] S. Goriely, N. Chamel, and J. M. Pearson, *Phys. Rev. C* **82**, 035804 (2010).
- [17] P. Raghavan, *At. Data Nucl. Data Tables* **42**, 189 (1989).
- [18] Y. Xu, S. Goriely, A. Jorissen, G. L. Chen, and M. Arnould [Astron. Astrophys. (to be published)].
- [19] B. B. Back, J. Bang, S. Björnholm, J. Hattula, P. Kleinheinz, and J. R. Lien, *Nucl. Phys. A* **222**, 377 (1974).
- [20] S. Goriely, *Phys. Lett. B* **436**, 10 (1998).
- [21] J. P. Jeukenne, A. Lejeune, and C. Mahaux, *Phys. Rev. C* **16**, 80 (1977).
- [22] E. Bauge, J. P. Delaroche, and M. Girod, *Phys. Rev. C* **63**, 024607 (2001).
- [23] E. Bauge, J. P. Delaroche, M. Girod, G. Haouat, J. Lachkar, Y. Patin, J. Sigaud, and J. Chardine, *Phys. Rev. C* **61**, 034306 (2000).
- [24] H. Scheit, F. Maréchal, T. Glasmacher, E. Bauge, Y. Blumenfeld, J. P. Delaroche, M. Girod, R. W. Ibbotson, K. W. Kemper, J. Libert, B. Pritychenko, and T. Suomijärvi, *Phys. Rev. C* **63**, 014604 (2000).
- [25] E. Bauge, J. P. Delaroche, and M. Girod, *Phys. Rev. C* **58**, 1118 (1998).
- [26] J. P. Jeukenne, A. Lejeune, and C. Mahaux, *Phys. Rev. C* **14**, 1391 (1974).
- [27] R. Capote *et al.*, *Nucl. Data Sheets* **110**, 3107 (2009).
- [28] S. Hilaire, J. P. Delaroche, and M. Girod, *Eur. Phys. J. A* **12**, 169 (2001).
- [29] S. Hilaire and S. Goriely, *Nucl. Phys. A* **779**, 63 (2006).
- [30] S. Goriely, S. Hilaire, and A. J. Koning, *Phys. Rev. C* **78**, 064307 (2008).
- [31] M. Igashira, Y. Nagai, K. Masuda, T. Ohsaki, and H. Kitazawa, *Astrophys. J.* **441**, 89 (1995).
- [32] J. Meissner, H. Schatz, J. Gorres, H. Herndl, M. Wiescher, H. Beer, and F. Kappeler, *Phys. Rev. C* **53**, 459 (1996).
- [33] T. Ohsaki, M. Igashira, Y. Nagai, M. Segawa, and K. Muto, *Phys. Rev. C* **77**, 051303 (2008).
- [34] H. Beer, P. V. Sedyshev, W. Rochow, P. Mohr, and H. Oberhummer, *Nucl. Phys. A* **705**, 239 (2002).
- [35] A. Tomyo, Y. Nagai, Y. Nobuhara, T. Shima, H. Makii, K. Mishima, and M. Igashira, *Nucl. Phys. A* **718**, 527 (2003).
- [36] J. Colditz and P. Hille, *Oesterr. Akad. Wiss., Math-Naturw. Kl., Anzeiger* **105**, 236 (1968).
- [37] D. J. Hughes, R. C. Garth, and J. S. Levin, *Phys. Rev.* **91**, 1423 (1953).
- [38] P. Mohr, H. Beer, H. Oberhummer, and G. Staudt, *Phys. Rev. C* **58**, 932 (1998).
- [39] K. H. Guber, L. C. Leal, R. O. Sayer, R. R. Spencer, P. E. Koehler, T. E. Valentine, H. Derrien, and J. A. Harvey, *J. Nucl. Sci. Tech. Suppl.* **2**, 346 (2002).
- [40] G. Calvi, R. Potenza, R. Ricamo, and D. Vinciguerra, *Nucl. Phys.* **39**, 621 (1962).
- [41] R. L. Henkel and H. H. Barschall, *Phys. Rev.* **80**, 145 (1950).
- [42] H. Beer, P. V. Sedyshev, Y. P. Popov, W. Balogh, H. Herndl, and H. Oberhummer, *Phys. Rev. C* **52**, 3442 (1995).
- [43] A. G. Dovbenko, V. E. Kolesov, V. P. Koroleva, and V. A. Tolstikov, *At. Energ.* **23**, 151 (1967).
- [44] P. Mohr, P. V. Sedyshev, H. Beer, W. Stadler, H. Oberhummer, Y. P. Popov, and W. Rochow, *Phys. Rev. C* **59**, 3410 (1999).
- [45] P. V. Sedyshev, Y. P. Popov, P. Mohr, H. Beer, H. Oberhummer, and W. Rochow, *Int. Sem. Int. Neutrons Nucl.* **6**, 205 (1998).
- [46] H. Beer, C. Coceva, P. V. Sedyshev, Y. P. Popov, H. Herndl, R. Hofinger, P. Mohr, and H. Oberhummer, *Phys. Rev. C* **54**, 2014 (1996).
- [47] S. Chiba, H. Koura, T. Hayakawa, T. Maruyama, T. Kawano, and T. Kajino, *Phys. Rev. C* **77**, 015809 (2008).